Polymer Degradation and Stability 166 (2019) 108–120

Contents lists available at ScienceDirect

Polymer Degradation and Stability

journal homepage: www.elsevier.com/locate/polydegstab

Atomic oxygen degradation mechanisms of epoxy composites for space applications

Yanjun He [a], Agnieszka Suliga [b], Alex Brinkmeyer [b], Mark Schenk [a], Ian Hamerton [a, *]

[a] Department of Aerospace Engineering, School of Civil, Aerospace, and Mechanical Engineering, Queen's Building, University of Bristol, University Walk, Bristol, BS8 1TR, UK
[b] Oxford Space Systems, Electron Building, Harwell Space Cluster, Harwell, OX11 0QR, UK

ARTICLE INFO

Article history:
Received 11 March 2019
Received in revised form
9 May 2019
Accepted 20 May 2019
Available online 23 May 2019

Keywords:
Epoxy resins
Atomic oxygen
Ultra-thin space composites
Thermoset polymers
Principal components analysis

ABSTRACT

The effects of atomic oxygen on three commercial composite materials, based on two space-qualified epoxy resins (tetraglycidyl-4,4′-diaminodiphenylmethane (TGDDM) cured with a blend of 4,4′-methylenebis(2,6-diethylaniline) and 4,4′-methylenebis(2-isopropyl-6-methylaniline); and a blend of TGDDM, bisphenol A diglycidyl ether (DGEBA), and epoxidised novolak resin initiated by N'-(3,4-dichlorophenyl)-N,N-dimethylurea) are studied. Samples were exposed to a total fluence of (3.82×10^{20}atom/cm^2), equating to a period of 43 days in low Earth orbit. The flexural rigidity and modulus of all laminates displayed a reduction of 5–10% after the first exposure (equivalent to 20 days in orbit). Fourier transform infrared (FTIR) spectra, obtained during prolonged exposure to atomic oxygen, were interpreted using multivariate analysis to explore the degradation mechanisms.

1. Introduction

Advanced composite materials are promising candidates in space applications, particularly those involving deployable structures and spacecraft structural components, due to their high specific stiffness and strength resulting from their low weight [1]. However, the high vacuum, extreme thermal cycling, vacuum ultraviolet (VUV) radiation, and the risk of atomic oxygen (AO) erosion [2], make the space environment a highly aggressive one: high vacuum (10^{-4}-10^{-5} Pa), UV (100–200 nm), thermal cycling (−150 to 150 °C), AO, charged particles, electromagnetic radiation, micrometeoroids, and man-made débris, severely limiting the durability of composite materials. When deployed in low Earth Orbit (LEO), satellites are particularly prone to AO exposure (with kinetic energy of 5eV, nominal AO flux of around 10^{14}-10^{15} atoms/cm^2 s), which plays a major role in the degradation of polymer based composite materials [3]. Several in-orbit tests have been performed by the European Space Agency (ESA) [4], Japan Aerospace Exploration Agency (JAXA), and the National Aeronautics and Space Administration (NASA) [5–8], to understand the AO resistance of various materials, and these have been reviewed [9]. Extensive research has been undertaken to investigate the AO resistance of composite materials using ground-based facilities, but few publications focus on the AO behaviour of space-qualified composites that are already used in orbit. Two kinds of AO are involved in the degradation mechanisms: the ground state (3P) and electronically-excited (1D) form [10]. The ground state form, O (3P), can abstract a hydrogen atom in the polymer structure to form a hydroxyl group with activation energies of 28.9 kJ/mol (where the hydrogen atom is primary), 18.8 kJ/mol (secondary), and 13.8 kJ/mol (tertiary) (Fig. 1).

It has been determined [10] that AO can attack benzene by two modes: abstraction of a hydrogen atom from benzene to form a hydroxyl radical and a phenyl radical, or addition of AO to form various possible products (Fig. 2).

The compounds vary in stability: I, II, III, and IV undergo

Abbreviations: AO, Atomic oxygen; LEO, Low earth orbit; VUV, Vacuum ultraviolet; ESA, European space agency; POSS, Polyhedral oligomeric silsesquioxanes; TGDDM, Tetraglycidyl-4,4′-diaminodiphenylmethane; DGEBA, Bisphenol a diglycidyl ether; FTIR, Fourier transform infrared; ATR, Attenuated total reflectance; DSC, Differential scanning calorimetry; TGA, Thermogravimetric analysis; DMTA, Dynamic mechanical thermal analysis; PCA, Principal components analysis; ISS, International Space Station; JAXA, Japan Exploration Aerospace Agency Japan; LDEF, Long duration exposure facility; MISSE, Materials international space station experiments; NASA, National Aeronautics and Space Administration; SEM, Scanning electron microscopy.

* Corresponding author.
E-mail address: ian.hamerton@bristol.ac.uk (I. Hamerton).

https://doi.org/10.1016/j.polymdegradstab.2019.05.026
0141-3910/

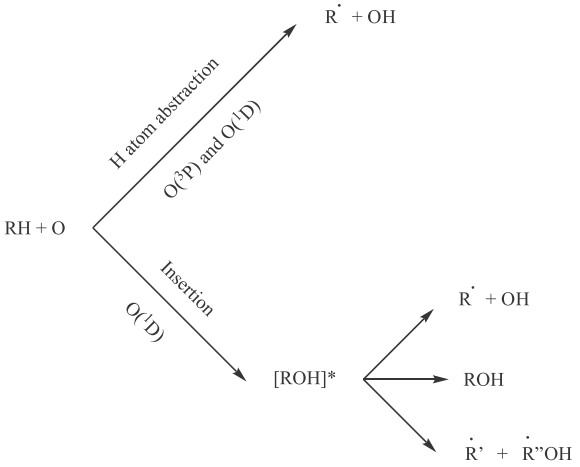

Fig. 1. Schematic showing the generic reactions followed by AO [11].

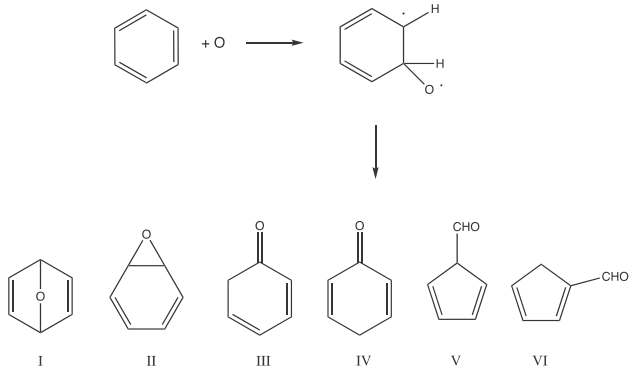

Fig. 2. Schematic showing the observed reactions between benzene and AO [10].

rearrangement to a more stable phenolic structure while V and VI are likely to undergo condensation and polymerisation reactions [10]. The excited form, O (1D), can also react with more complex aromatic compounds by abstraction, but is more likely to undergo insertion into the C—H bond of an alkyl substituent with no energy barrier. The reactions between AO and such aromatic compounds are more complex than benzene meaning that the degradation mechanisms are specific to particular substituents.

Epoxy resins are the most commonly used composite matrices in satellite applications [12], with a range of space-qualified resins now commercially available. Those used in this study are shown in Fig. 3, where both aromatic rings and alkyl moieties can be seen. The principal reaction that the epoxy matrices undergo with AO is believed to be through the biphenyl segment containing a saturated alkyl bridge between the phenyl rings of the epoxy, and the alkyl substituents. During the reaction, volatile fragments, such as short-chain oxidation products, may leave the surface and thus degrade the performance of the materials. This surface degradation is particularly detrimental for deployable structures, which rely on material compliance for compact stowage during launch, by bending and folding ultra-thin composite laminates [13,14]. Various techniques have been studied to increase the AO resistance of materials in LEO. Among these techniques, AO resistant coatings are the most commonly used. This technique provides a barrier for space materials against the AO environment and different coatings have been widely studied in Long Duration Exposure Facility (LDEF) experiment [15,16]. The patented Photosil™ surface modification process incorporates silicon-containing chemical groups into the

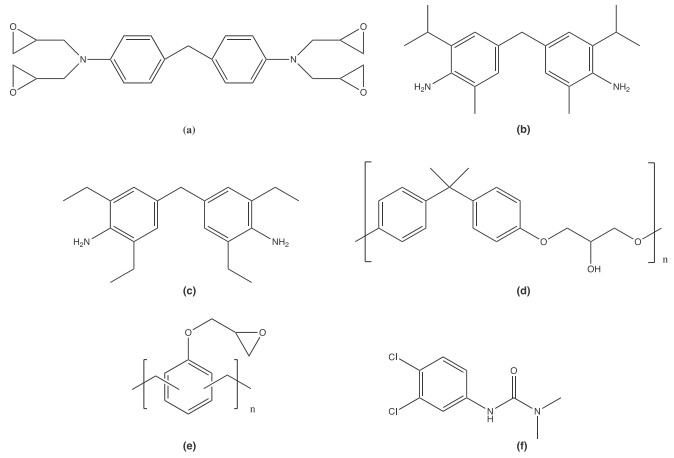

Fig. 3. Chemical structures of epoxy resin A: (a) TGDDM cured with (b) 4,4′-methylenebis(2,6-diethylaniline) and (c) 4,4′-methylenebis(2-isopropyl-6-methylaniline); and epoxy resin B: (a) TGDDM, (d) DGEBA, and (e) epoxidised novolak resin initiated by (f) N'-(3,4-dichlorophenyl)-N,N-dimethylurea).

sub-surface layer (*i.e.* up to 1 μm in depth) of the polymer coating. Kleiman et al. [17] reported that this technique can increase the AO resistance without a significant reduction in the thermo-optical properties or mechanical properties of the treated materials, but the high surface strains during stowage and deployment of the structures preclude the use of coatings or shielding that are conventionally employed to protect composite materials in orbit. Polymer modification using chemical means, generally involving the incorporation of silicon atoms through oligosiloxanes chain segments [18] or polyhedral oligomeric silsesquioxanes (*i.e.* POSS reagents), has been studied by a number of researchers to promote the AO resistance of space materials [12,19] and work going in our laboratories is also focused on both approaches.

In the present paper, the degradation mechanism of three commercial composites materials is studied in detailed using principal components analysis (PCA) to provide guidelines for the design of new resin system. PCA has been widely used to study the degradation of polymers. To date, few studies have been conducted to examine the AO erosion of polymers using PCA. Awaja et al. are notable exceptions, as their work examined the surface degradation of glass fibre-reinforced epoxy [20] and carbon-fibre reinforced epoxy nanocomposites [21] using a combination of X-ray photoelectron spectroscopy (XPS), time of flight secondary ion mass spectrometry (ToF-SIMS), and scanning electron microscopy. Their approach used PCA to differentiate the elemental data in terms of the concentrations of molecular species produced by the exposure conditions. There are some similarities in the epoxy studied by Awaja et al. (a difunctional epoxy) and epoxy B in this work, and so the ensuing discussion takes account of the degradation species reported in the literature study.

In the present work, the effects of AO exposure on the mechanical properties of three thin laminates, based on two commercial space-qualified resins, are exposed in three successive cycles, and their mechanical, chemical, and surface properties assessed after each cycle. The three laminates examined in this work are designed for space applications and employ two highly crosslinked polymer matrices yielding high glass transition temperatures. Furthermore, the different polymerisation mechanisms (featuring an amine-cured reaction, and a polyetherification reaction) yield different structures after cure which allows comparison of the mechanisms of degradation. The flexural rigidity of thin laminates was expected to be particularly sensitive to surface

erosion due to AO and was therefore selected to as a parameter to monitor any change in mechanical properties. The test protocol consisted of applying a three-point bend test in the elastic region, subsequently exposing the sample to atomic oxygen, and finally performing the three-point bend test again to assess the change in flexural properties, while the surface morphology was determined after each exposure. Vibrational spectroscopy, coupled with multivariate analysis, was employed to explore the degradation mechanisms experienced by the polymer matrices. The insights gained into the degradation mechanism will aid the design of a new resin system for improved AO resistance.

2. Experimental methods

2.1. Materials

Two commonly used resin systems for commercial applications (supplied by Solvay, UK), are used in this work. They are well characterized by their high glass transition temperature (T_g), thermal stability, and high modulus. The chemical structures of the constituent components are shown in Fig. 3.

The laminates formed from these resins, along with the designations used, are shown in Table 1. Laminate LAM01 uses a resin system (Epoxy A) which contains (a) tetraglycidyl-4,4′-diaminodiphenylmethane (TGDDM) cured with a blend of (b) 4,4′-methylenebis(2,6-diethylaniline) and (c) 4,4′-methylenebis(2-isopropyl-6-methylaniline). Laminates LAM02 and LAM03 use the same resin system (Epoxy B), which is formulated from a blend of three epoxy resins: (a) TGDDM, (d) bisphenol A diglycidyl ether (DGEBA), and (e) an epoxidised novolak resin, initiated by (f) N'-(3,4-dichlorophenyl)-N,N-dimethylurea).

2.2. Curing procedure

Epoxy A followed a two-step cure suggested by the supplier [22]: the sample was heated at 2 K/min. before being held isothermally at 130 °C (2 h) and heated again to 180 °C before being held isothermally (2 h). Following cure, the samples were cooled to 60 °C at a rate of -3K/min. Epoxy B also employed a two-step cure suggested by the supplier [23]: initial curing was performed at 135 °C for 1 h at 0.62 MPa pressure while a free-standing post cure was employed at 180 °C for 1 h.

2.3. Exposure test

The AO exposure test was carried out using a radio-frequency plasma asher, located in the Department of Physics, University of Bristol. The plasma was generated in a glass tube (length 300 mm, diameter 105 mm) and the samples were placed within the chamber, on an aluminium panel. The pressure in the main chamber was 100 Pa while gaseous oxygen was pumped into the chamber at around 0.2NL/min; here NL/min refers to "normal litres per minute" and represents the oxygen flux, calculated back to 'normal' conditions: 0 °C, 1 atm (101.3 Pa). AO fluence was calculated based on the mass loss of a reference Kapton™ H polyimide sample using equation (1) [24].:

$$F = \frac{M_k}{\rho_k A_k E_k} \tag{1}$$

where F is the AO fluence (atom/cm^2), ΔM_k is the mass loss of Kapton™ H film (g), ρ_k is the density of Kapton™ H (g/cm^3), A_k is the area of Kapton™ H film (cm^2), and E_k is the erosion yield of Kapton™ H (cm^3/atom), which is a constant (3×10^{24}cm^3/atom) measured in the LEO environment [24]. Once the AO fluence was calculated, the erosion yield of tested samples can be calculated using equation (2):

$$E_y = \frac{M}{\rho A F} \tag{2}$$

where E_y erosion yield of tested sample (cm^3/atom), ΔM is the mass loss of tested sample (g), ρ is the density of tested sample (g/cm^3), A is the sample surface area (cm^2), and F is the AO fluence (atom/cm^2) calculated using equation (1).

The cumulative AO fluence received in each exposure run and its equivalent duration in orbit is shown in Table 2. The equivalent duration in orbit of each exposure was calculated based on the data from a mission in International Space Station (ISS) launched on June 2001, when the sun entered a period of high activity. During this period the AO fluence in ISS was also maintained at a high level, the total AO fluence of this missions is $3.28 \cdot 10^{21}$ atom/cm^2 for one year of exposure [24].

2.4. Characterization methods

Surface morphology. The laminate surfaces were investigated before and after exposure using a Hitachi TM3030Plus table-top microscope (accelerating voltage 15 kV).

Differential Scanning Calorimetry (DSC). DSC was performed on cured laminates under flowing nitrogen (40 cm^3/min) using a TA Instruments Q200. Samples (*ca.* 10 mg) were cut and placed in a hermetically sealed aluminium pan. Each sample was then subjected to a heat/cool/heat analysis. First heating ramped from room temperature to 300 °C at a rate of 10 K/min while the second heating use the same ramping rate to determine the glass transition temperature (T_g).

Thermogravimetric analysis (TGA). TGA was performed using a TA Instruments Q500 apparatus on the cured (unexposed) laminates. Laminate samples (*ca.* 8 mg) were placed in an open platinum crucible and heated from room temperature to 600 °C with a ramp rate of 10 K/min. in flowing nitrogen (40 cm^3/min) to degrade the matrix, and then heated from 600 °C to 1000 °C with the same ramp rate in air to burn the fibre off.

Thermo-mechanical properties. Dynamic mechanical thermal analysis (DMTA) was performed in single cantilever mode at an amplitude of 15 Hz on each sample (0.3 mm × 12 mm × 36 mm) using a TA Instruments Q800. Five specimens of each laminate were tested by heating at a rate of 10 K/min. from ambient temperature to 250 °C.

Spectroscopic analysis. Analysis of the surfaces of the laminates,

Table 1
The laminates used in this work.

Designation	Laminate description	Lay-up (woven fabric)
LAM01	Carbon fibre reinforced epoxy resin A	(±45/0/±45)[a]
LAM02	Carbon fibre reinforced epoxy resin B	$(0/90)_3$
LAM03	Carbon/Kevlar fibre reinforced epoxy resin B	(±45/0/90/±45)[b]

[a] The middle ply contains unidirectional carbon fibres.
[b] The top and bottom plies comprise woven carbon fibre, while Kevlar forms the middle ply.

Table 2
AO fluence for each exposure.

Test performed	Exposure cycle	Exposure duration (hr)	Total AO fluence ($\times 10^{20}$ atom/cm^2)	Equivalent duration in orbit (days)
Three-point bend and SEM	1	3	1.75	20
	2	3	2.82	31
	3	3	3.82	43
FTIR analysis	1	1	0.26	3
	2	1	0.66	8
	3	1	0.84	10
	4	1	1.02	12
	5	1	1.25	14
	6	1	1.60	18

which had been progressively exposed to AO (over six cycles, total AO fluence *ca.* 1.6×10^{20}atom/cm^2), was performed under ambient conditions after each exposure to AO using a Perkin–Elmer Series 2000 Fourier transform infrared (FTIR) spectrometer with a diamond attenuated total reflectance (ATR) accessory; the AO fluence for each cycle is shown in Table 2.

2.5. Three-point bend test

The three-point bend test was conducted on Shimadzu mechanical test machine with a 1 kN load cell, following procedure A of the ASTM D790-15 standard [25]. The ASTM standard recommends a span to thickness ratio of 16:1. However, Zweben et al. [26] reported that for thin samples, the span to thickness ratio should be more than 60:1 to obtain an accurate result. Thus, the laminates were cut into five 38 mm × 14 mm test specimens (Table 3) and a span of 22 mm was used.

The main output of these tests is the effective flexural modulus, equation (3) [25]:

$$E = \frac{P\,L^3}{4\,b\,t^3\,\delta} \tag{3}$$

where E is the effective flexural modulus (GPa), P is load (N), L is the support span (m), δ is the deflection of the centreline of the specimen at the middle of the support span (m), b is the width of specimen tested (m), and t is the thickness of beam tested (m).

Flexural modulus has been used to examine the flexural properties in most of the literature cited. However, in this work, it is hard to characterize flexural properties since the magnitude of flexural modulus is affected by the thickness of the laminate sample and, as this parameter displayed some variation (Table 3) and will change with AO exposure. Thus in addition to flexural modulus, the flexural rigidity [26], calculated using equation (4), was also used to characterize the flexural properties of each laminate

$$EI = \frac{P\,L^3}{48\,\delta} \tag{4}$$

where EI is the flexural rigidity (Nm^2), P is load (N), L is the support span (m), and δ is the deflection of the centreline of the specimen at the middle of the support span (m).

Table 3
Dimensions of all samples tested.

Sample designation	Width (mm)	Length (mm)	Thickness (mm)
LAM01	13.80	38.38	0.25
	13.43	38.62	0.24
	13.85	38.20	0.25
LAM02	13.20	36.74	0.32
	13.17	37.47	0.34
	13.13	37.25	0.33
LAM03	13.75	38.47	0.40
	13.64	37.80	0.38
	13.95	38.91	0.39

2.6. Principal components analysis

The FTIR data were studied using PCA, which is a multivariate analysis technique that is widely used to study the changes in shift or intensity of spectroscopic data [27–29]. The technique provides a mathematical transformation of the raw data to reduce the dimensionality of the data, thus allowing a better assessment of the differences and similarity of the spectra between various samples. The matrix equation of the PCA model is shown in equation (5):

$$\boldsymbol{X} = \boldsymbol{T}\,\boldsymbol{P}^{\boldsymbol{T}} + \boldsymbol{E} \tag{5}$$

where $\boldsymbol{T}$ is the scores matrix, $\boldsymbol{P}$ the loadings matrix and $\boldsymbol{E}$ the error matrix [27]. In this work, the $\boldsymbol{X}$ matrix represents the raw FTIR data before and after different exposures, and the $\boldsymbol{T}$ and $\boldsymbol{P}$ matrices were generated by the PCA model, which was built using MATLAB software.

3. Results and discussion

3.1. Baseline results before exposure

Several chemical and mechanical tests were performed on the unexposed laminates to provide a baseline (Table 4) to compare with the performance after exposure. The mechanical properties of the three laminates vary due to the different resin systems and layups used. LAM01 and LAM02 have comparable glass transition temperatures (T_g), since the structures of the two resins and the two laminate configurations are similar. LAM03 used a different fibre in the middle ply, which leads to a lower T_g value compared to the other two laminates.

The mechanical loss angle tangent data (tan δ) are shown as a function of temperature in Fig. 4. The tan δ response reflects the energy loss and viscous behaviour of the material (*i.e.* the damping capability), which is determined by the epoxy matrix and the interface between resin and fibres.

LAM01 employs a different resin compared with the other two laminates and has a higher tan δ value than other two laminates, which indicate that there is more energy dissipated within epoxy A. LAM02 and LAM03 use the same resin system, with the difference in the tan δ peaks attributed to the difference in the interface between fibre and matrix. A stronger fibre/matrix interface can result in a lower peak height [30]. Thus, the results suggest that the interface between the rigid (and non-reactive) thermoplastic polyamide Kevlar™ and epoxy is stronger than the interface between carbon fibre and the epoxy. The TGA data for all three laminates are shown in Fig. 5.

LAM 01 has the highest fibre volume fraction of the laminates tested. The resin systems in all laminates were completely burned

Table 4
Chemical and mechanical properties of laminates before exposure.

Laminates	Flexural rigidity/N*m^2	Flexural modulus/GPa	T_g/°C		
			E''_{max}	tan δ_{max}	DSC
LAM 01	441.4 ± 19.2	25.8 ± 1.1	211	224	187
LAM 02	461.4 ± 18.2	11.7 ± 0.6	213	215	167
LAM 03	467.3 ± 26.6	6.9 ± 0.2	199	204	161

Key: $E''_{max} = T_g$ determined from the peak maximum in the loss modulus response; tan $\delta_{max} = T_g$ determined from the peak maximum in the tan δ data; DSC = T_g determined from DSC rescan data.

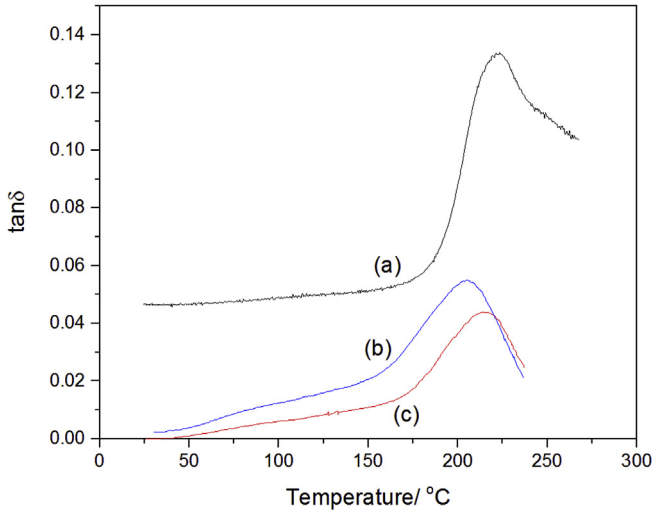

Fig. 4. Mechanical loss angle tangent (tan δ) as a function of temperature for (a) LAM01, (b) LAM02, and (c) LAM03.

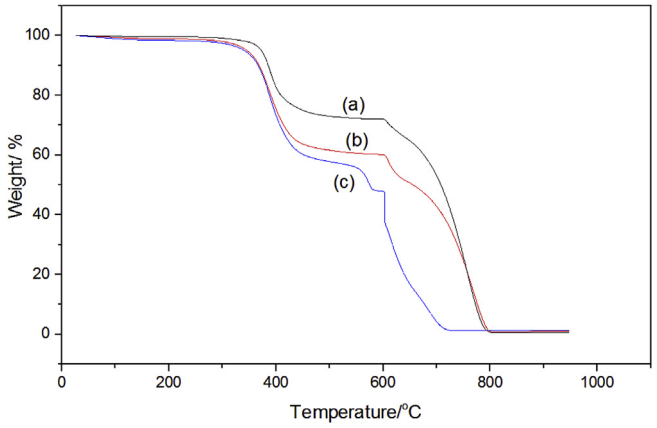

Fig. 5. TGA data for (a) LAM01, (b) LAM02, and (c) LAM 03.

off at around 450 °C and Kevlar™ in LAM 03 also start to degrade after around 500 °C. After 600 °C, the gas was switched from nitrogen to air and the carbon fibres start to degrade. A detailed outline of the mass loss with the increase in temperature is shown in Table 5.

3.2. Three-point bend

The three thin laminates were exposed in three successive cycles of AO exposure (Table 2), and their flexural properties were assessed after each cycle. The mechanical properties are shown as a function of AO fluence in Fig. 6. Both the flexural rigidity and

Table 5
Mass loss of the laminates as a function of temperature.

Laminates	temperature [°C] at which weight loss [%] recorded					
	100	200	300	400	500	600
LAM01	0.2	0.4	1.0	17.7	27.1	28.1
LAM02	0.6	1.1	2.0	24.5	38.4	39.8
LAM03	1.0	1.6	2.5	26.2	42.2	52.1

modulus of all laminates displayed a reduction of around 5% after the first exposure, due to the erosion of the matrix resin; this reduction in flexural properties will be particularly significant for the thin laminates considered here. Although the laminates displayed a general reduction in mechanical properties as a function of AO exposure, LAM01 and LAM03 displayed an increase in the flexural modulus after the third exposure. At this stage, based on five replicate samples there is reasonable evidence to suggest that following exposure the flexural properties initially fall and may recover slightly. However, the results of the data are not unequivocal and the data set would need to be increased significantly to verify this and provide better statistical confidence in the variation in the mechanical properties.

This would, in turn, be carried out in future work, and does not invalidate the results of this study, which is focused on the degradation of the matrices. If the observation is correct and generally representative of other materials, then it is likely that the phenomenon would be due to additional crosslinking of the carbon fibres (graphitisation) and probably has some aspects in common with recent work published on pyrolysed cyanate esters [31], where mechanical performance and resilience (as evidenced by nanoindentation) were markedly increased. However, the experiments were not designed to explore this explicitly and will form the basis of a future, more specific study.

According to data acquired in-orbit during NASA's Materials International Space Station Experiments (MISSE) programme [24], the resin matrix is significantly more susceptible to the effects of AO than the reinforcing fibres: the erosion yield of epoxy is about 10 times greater than that recorded for pyrolytic graphite (a model for the carbon fibres). Thus, after the majority of the surface resin has been eroded, the exposed carbon fibre is relatively resistant to erosion, although not entirely inert. Therefore, after the first exposure, the flexural properties will not change significantly unless the fibres become seriously eroded and damaged, which requires a higher AO fluence than is achieved in this work.

3.3. Surface morphology

Samples were examined using SEM to determine the effects of AO exposure on the surface morphology. Before the samples had been undergone AO exposure, no obvious defects were detected on the surface of three laminates (Fig. 7 (a), (c), and (e)). AO is highly aggressive towards organic materials, as evidenced by the SEM analysis: after the third exposure, when all samples had received

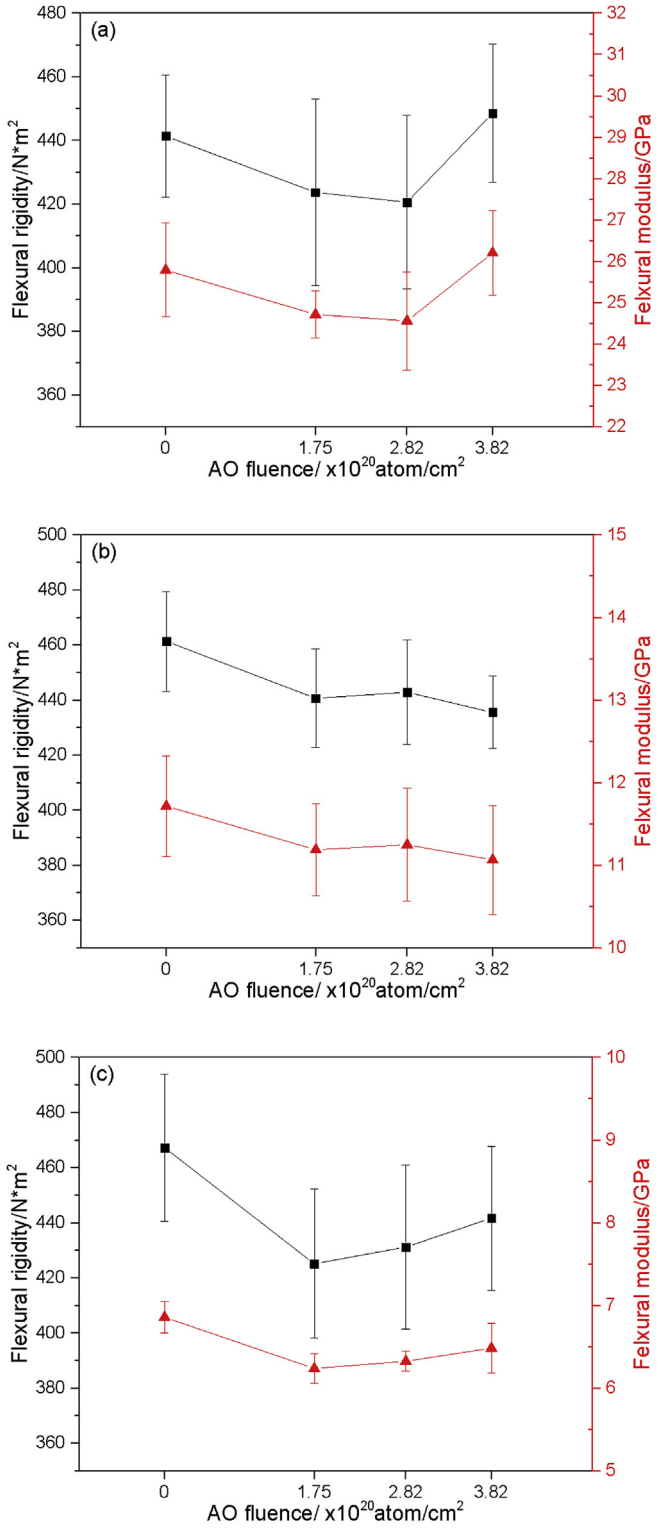

Fig. 6. Flexural properties of (a) LAM01, (b) LAM02 (middle), and (c) LAM03 as a function of AO fluence exposure (—■— = flexural rigidity, —▲— = flexural modulus).

the highest total AO fluence, the surface resins had been severely eroded from all the laminates, exposing the underlying fibres to the AO (Fig. 7 (b), (d), and (f)). In addition to the resin erosion, it is also noticeable that the resin in the gaps between the fabric yarn in LAM01 displays significant cracks after AO exposure (Fig. 7 (b)), which are not present in either LAM02 or LAM03.

However, even at low AO exposure, a significant amount of surface resin had been removed to reveal the carbon fibres, *i.e.* even after the first cycle (Fig. 8(a)). A gradual erosion of the surface resin is shown for LAM03, where the surface resin was further eroded in the second exposure (Fig. 8(b)), while in the third exposure the surface resin had been almost completely eroded (Fig. 8(c)).

3.4. FTIR spectroscopy

The SEM data (Fig. 7) show that the pattern of erosion is uneven, evidenced by the "pitting" seen in the residual resin, which is located in the gaps and at the edges between the warp and weft of the carbon fibre yarns in each laminate. These small holes indicate that the erosion due to AO is not uniform, and it occurs at weaker points in the resin (*e.g.* at structural moieties which are more susceptible to attack such as hydrogen atoms bonded to alkyl fragments) and provides a path for AO to erode the underlying resin still further. A study was carried out using spectral analysis, coupled with multivariate analysis, to explore the chemical nature of the degradation mechanism.

The reaction between the polymer matrices and AO is complex and depends on the chemical nature of the matrices. In this work, two different resin systems were used. Epoxy A with the TGDDM is highly aromatic, highly crosslinked, and the epoxy is tetrafunctional, with glycidyl amine groups containing no methyl groups. The curing agents are aromatic with alkyl substituents. The second formulation, Epoxy B, contains the same tetrafunctional epoxy with a difunctional epoxy based on bisphenol A. However, this second epoxy has two key differences: it contains an isopropyl bridge, which incorporates the less stable methyl group, and is a low molecular weight oligomer (n = 0–1) which contains the less stable methylene and methyne moieties. The curing agent (a chlorinated aromatic compound containing both amide and tertiary amine functional groups) leads to a highly crosslinked network. These chemical differences offer potential for the degradation to follow different mechanistic pathways and spectral analysis is employed to probe this.

3.4.1. Spectral assignments

FTIR data, acquired for two resin systems before exposure, are shown in Fig. 9. As indicated in Section 2.1, the structures of the two cured resin systems contain many common functional groups, and thus the FTIR spectra show strong similarities. Several variations still exist due to the differences in the chemical structures caused by different epoxy resin and curing agent. The inset in Fig. 9 shows a peak fitting of the C–H stretching vibrations in the region of 3000-2850 cm^{-1} for each resin system; more alkyl species can be observed in LAM 01, which leads to a more complex C–H stretching region in 3000-2850 cm^{-1}. The two peaks present in 1740-1661 cm^{-1} in epoxy B are assigned to the C=O stretching vibration of the amide group, while epoxy A also shows strong peaks at that wavenumber which may be assigned to C=O stretch. However, this functional group does not exist in the structure of epoxy A, which may be assigned to an unknown component in epoxy A arising from manufacture. The intense band at around 800 cm^{-1} in epoxy B is assigned to the strongly dipolar C–Cl stretch, which is not present in epoxy A. The detailed assignments of the FTIR spectra are shown in Table 6; these will be applied as a baseline to study any peak changes after exposure to different levels of AO fluence.

3.4.2. Exploring the degradation mechanism of epoxy A using PCA

Fig. 10 shows the FTIR data of LAM01 as a function of AO fluence exposure (the results from the third exposure were removed due to an instrument error). The intensity of most peaks shows a decreasing trend after exposure and the CH stretching vibration

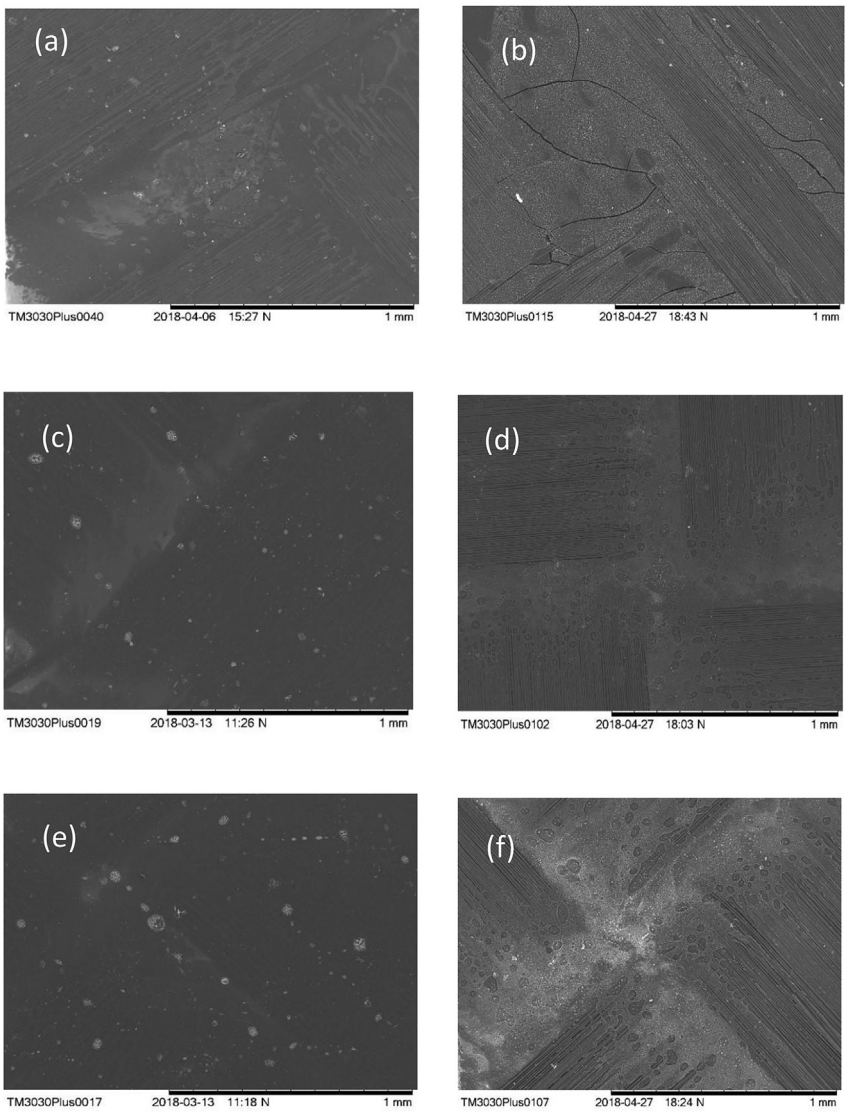

Fig. 7. The surface morphologies of LAM01 (a, b), LAM02 (c, d), and LAM03 (e, f) before and after third exposure (a, c, e, AO fluence = 0; b, d, f, AO fluence = 3.82×10^{20}atom/cm^2).

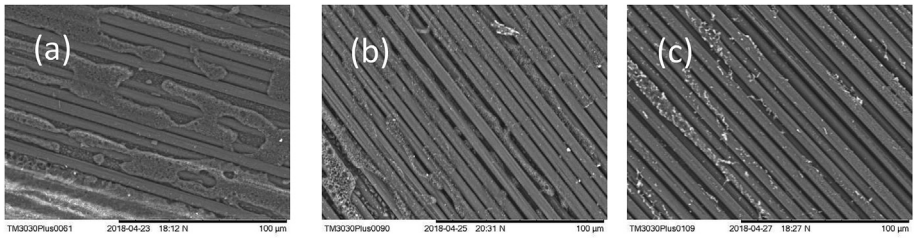

Fig. 8. The surface morphology of LAM03 following (a) first exposure, (b) second exposure, and (c) third exposure.

around 3000 cm^{-1} almost completely degraded after the fifth exposure. Only one peak, at around 1400 cm^{-1}, increased due to the formation of the O–H functional group (this is an O–H bend). However, it is hard to examine the AO performance of different structural moieties directly from the FTIR data. To better understand the degradation mechanism, PCA was applied to the FTIR data to study the effect of AO on the different functional groups of the two resins. The FTIR data will be input into PCA model as the matrix X in Equation (5).

To further understand the change with exposure, the data set was extracted using the PCA technique and the results are shown in Fig. 11.

The cumulative eigenvalue of each component in Fig. 11(a) shows that five components were obtained. The first three components represent around 98% of the overall FITR data set, thus, only PC1, PC2, and PC3 were analyzed. Fig. 11(b) and (c) show a change in the score, which refers to the matrix T in Equation (5), of each component as a function of exposure: the score of PC1

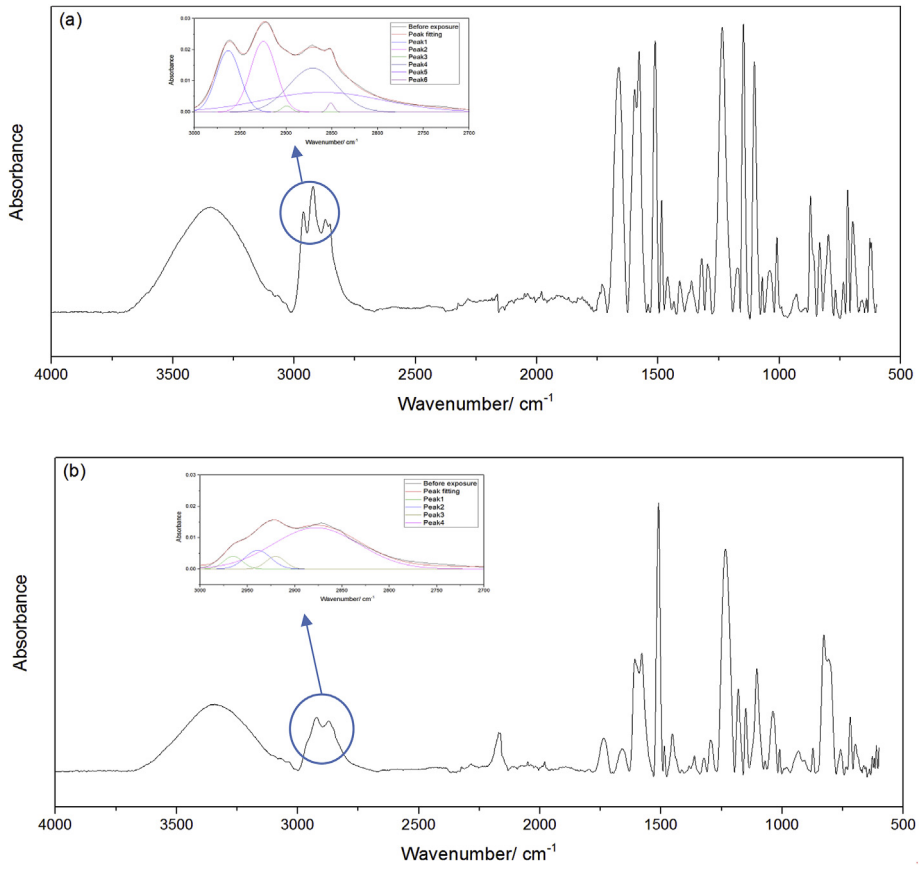

Fig. 9. FTIR data for (a) epoxy A and (b) epoxy B before exposure (insets show the CH stretching vibration region with fitted peaks).

Table 6
Spectral assignments of the two epoxy types used in this study.

Wavenumber/cm^{-1}	Functional group	Epoxy A	Epoxy B
3340	O–H stretching vibrations	✓	✓
3000–2850	C–H stretching vibration	✓	✓
1740–1660	C=O stretching vibration of unknown component	✓	
1740–1720	C=O stretching vibration		✓
1661	C=O stretching vibration		✓
1610–1450	Ring –C=C- stretching vibration	✓	✓
1461–1455	C–H deformation vibration	✓	✓
1420–1411	O–H deformation vibration	✓	✓
1362	C–H wagging vibrations of secondary alcohols	✓	✓
1320–1296	C–N stretching vibrations	✓	✓
1240–1170	=C–H in-plane deformation	✓	✓
1150–1075	C–O stretching vibrations	✓	✓
1040	C–O–C stretching vibrations		✓
1010	C–O stretching vibrations		✓
900–650	Ar ring vibrations	✓	✓
800	C–Cl stretching vibrations		✓

decreased with the increase of AO fluence. The score of PC2 increased after the first exposure and then started to decrease (it is worth noting that the score of PC2 before exposure was the lowest); both PC1 and PC2 offered a good means of separating the samples on the basis of exposure, while PC3 was less useful in differentiating the samples. Combining the trend of scores and loadings (refer to the matrix *P* in Equation (5), expressed as a percentage) of each PC, it can be concluded that PC1 is correlated with the overall change in the intensity of each peak, a positive value in the loading plot (Fig. 11(d)) suggesting a decrease in that peak, while the negative value indicates an increase.

PC2 represents the changing rate of each peak, thus a positive value indicates a gradual decrease in the intensity and a negative value indicates a significant decrease. For those wavenumbers where the PC2 loading is higher than PC1 this suggests that the intensity remains constant or increases following the early exposure, and decreases as the exposure progresses. PC3 represents the shift and the presence of newly-formed peak as the AO fluence

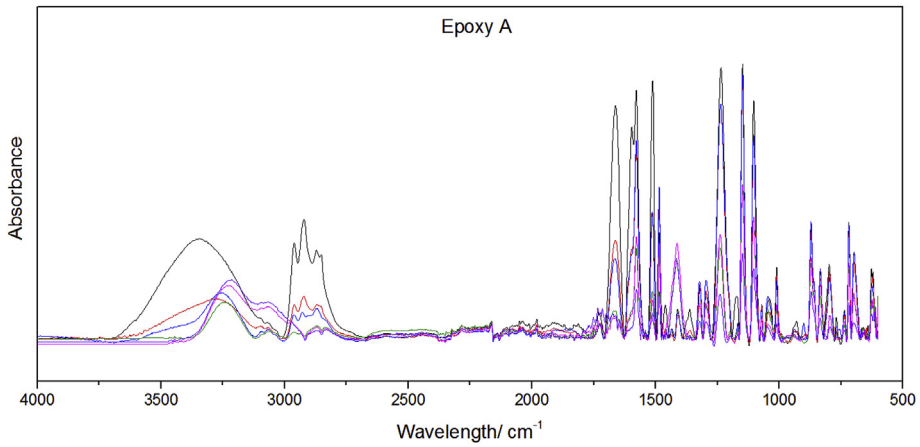

Fig. 10. FTIR spectra of epoxy A as a function of AO fluence exposure.

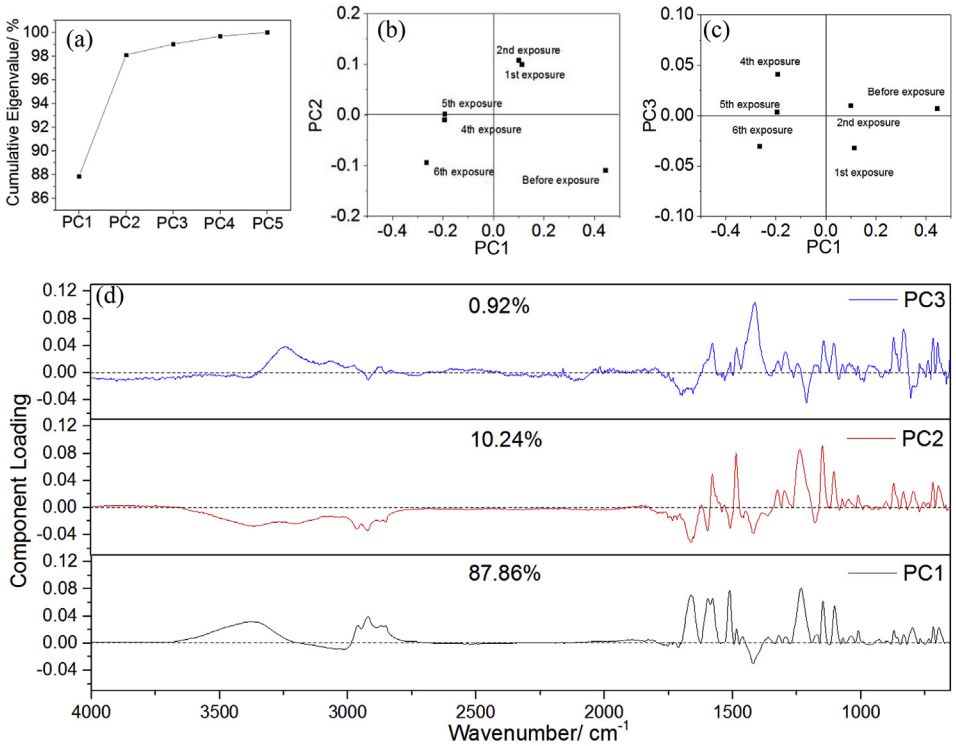

Fig. 11. PCA of FTIR spectra of epoxy A as a function of AO fluence exposure. (a) cumulative eigenvalue of each component (b) scores plot of PC1 *vs.* PC2. (c) scores plot of PC1 *vs.* PC3. (d) loading plot of PC1, PC2, and PC3.

increases. It is worth noting that the scores of PC1 and PC2 after first and second exposures, and the third and fourth exposures are similar while PC3 varies, which indicates that the changes from first exposure to second exposure, and from third exposure to fourth exposure are dominated by peak shift and formation instead of intensity change. The results of PCA study indicated several chemical or structural changes taking place during the erosion of epoxy A (and these are shown schematically in Fig. 12): the alkyl component degraded quickly during the reaction with AO, thus the intensity of the methyne CH group decreased sharply. The reaction between the AO and the methyne CH formed a number of hydroxyl and carboxyl groups, leading to an increase in the intensity of the O–H deformation vibration (1418 cm^{-1}) as a function of exposure. The O–H stretching vibration decreased in the early stages of exposure and then shifted to lower frequency due to the formation of different types of O–H (*i.e.* polymeric, hydrogen-bonded species).

The formation of the carboxylic functional group also leads to a shift in the O–H group (the carboxylic acid moiety may dimerise easily) and accounts for the formation of the C–O group. The aromatic –C=C- stretching vibration at 1595 cm^{-1} and the = C–H in-plane deformation in 1236-1173 cm^{-1} also decreased sharply due to the change in the distribution of aromatic substitution following AO reaction. The aromatic –C=C- stretching vibrations at 1511 cm^{-1} and 1486 cm^{-1} correlate with the both electronic donor and acceptor substituents in the aromatic ring. When the materials react with AO, the donors decreased and acceptors increased, thus the intensity at 1511 cm^{-1} decreased significantly while intensity at 1486 cm^{-1} increased during the early stages of exposure. Several peaks, such as the C–N stretching vibration at 1296 cm^{-1}, remained

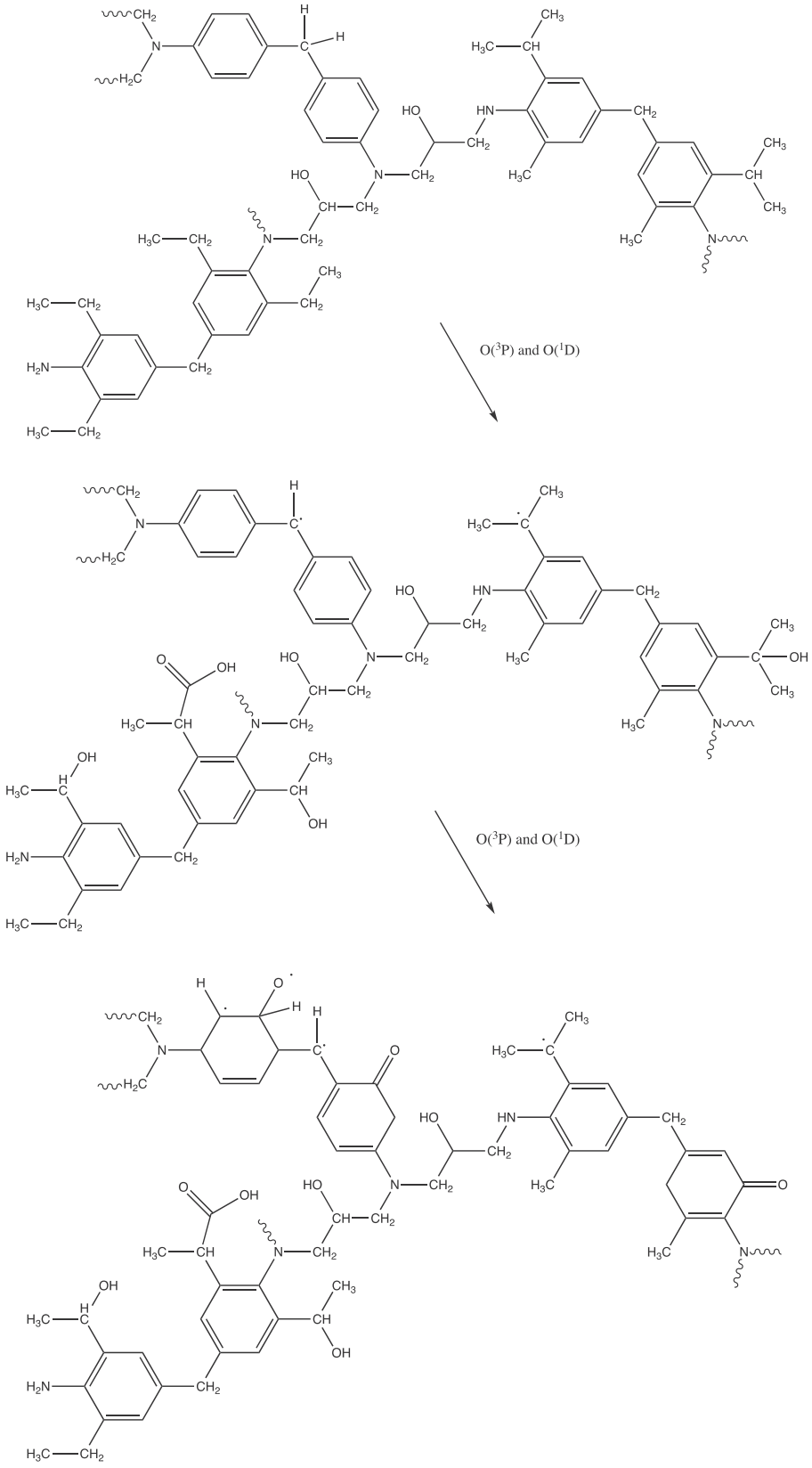

Fig. 12. Schematic showing range of potential degradation reactions when epoxy A is exposed to atomic oxygen.

Table 7
Summary of the change trend for each peak in epoxy A.

Intensity Trend	Wavenumber/cm^{-1}
Decreased sharply	3005-2673, 1664, 1595, 1512, 1460, 1362, 1173, 770
Decreased gradually	1578, 1360, 1233, 1103, 1071, 1043, 1010, 960-650
Increased in early exposure	1484, 1449, 1296, 871, 718, 679
Moderately increased	1418
Peak shifted/newly formed	3239, 3070, 2831

unchanged at the early stages of exposure, but began to decrease in intensity as exposure continued. These groups are less reactive with AO in the early stages but will finally experience degradation as the AO fluence increases. A summary of the trend in the changes observed for characteristic peaks is shown in Table 7.

These data are consistent with the study performed by Awaja et al. [20] who reported that increasing exposure to LEO conditions led to rapid formation of C–O, carbonyl and carboxyl species, indicating evidence of chain scission; erosion of the surface resin was also particularly evident. The aliphatic hydrocarbon

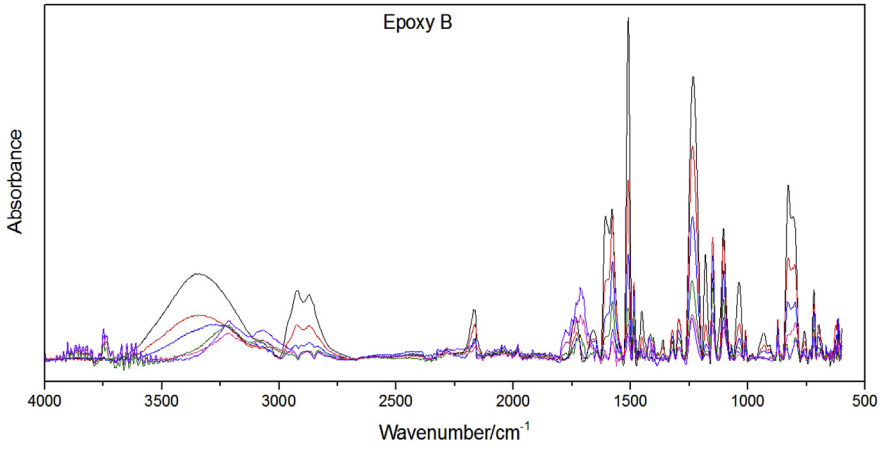

Fig. 13. FTIR spectra of LAM02 as a function of AO fluence exposure.

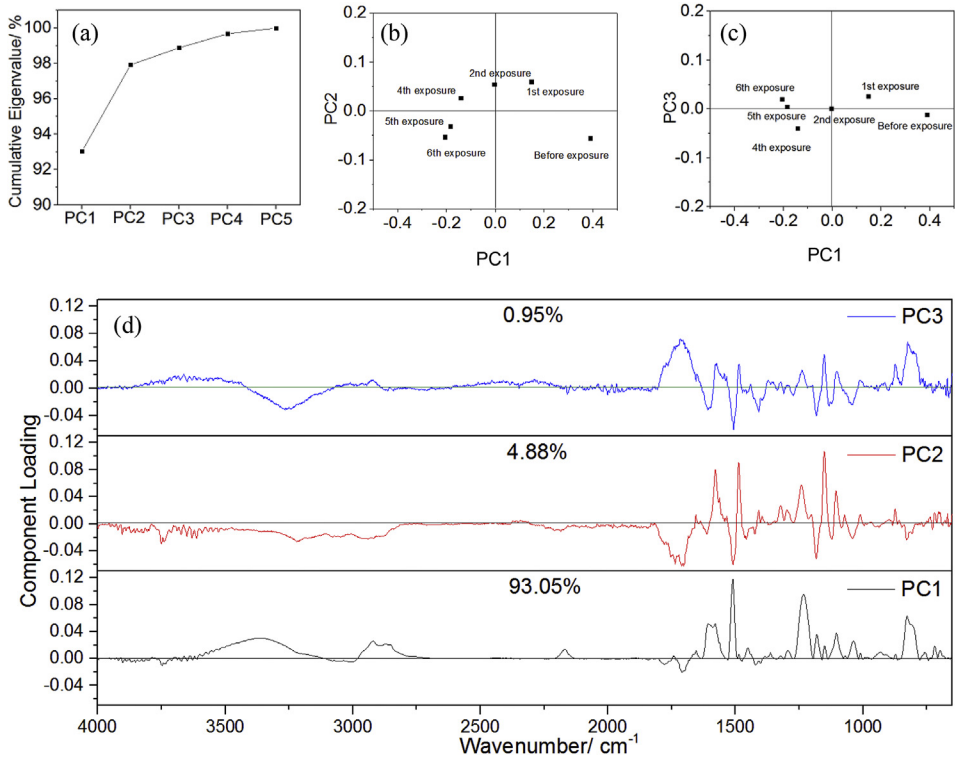

Fig. 14. PCA of FTIR spectra of LAM01 as a function of AO fluence exposure (a) cumulative eigenvalue of each component, (b) scores plot of PC1 *vs.* PC2, (c) scores plot of PC1 *vs.* PC3, (d) loading plots of PC1, PC2, and PC3.

Table 8
Summary of the change trend for each peak in epoxy B.

Intensity Trend	Wavenumber/cm^{-1}
Decreased sharply	2994-2687, 1610, 1509, 1455, 1182, 1121, 1081, 1039, 935, 829, 801, 700
Decreased gradually	1655, 1580, 1320, 1295, 1238, 1104, 1010, 871
Increased in early exposure	1485, 1149
Moderately increased	1740, 1423
Peak shifted/newly formed	3343, 2920-2850

components in the epoxy matrix (based on a bisphenol A/bisphenol F blend) were also susceptible (significant amounts of $C_3H_7NO^+$ were detected using ToF-SIMS, but positively-charged C2–C4 fragments were also evident).

3.4.3. Exploring the degradation mechanism of epoxy B using PCA

The corresponding FTIR data for epoxy B as a function of AO fluence exposure (Fig. 13) show a similar decreasing trend after exposure (the result of third exposure was removed due to an instrument error).

The data were also imported into PCA model as matrix *X* in Equation (5) to analyse the structural changes in epoxy B with increasing AO fluence and the results are shown in Fig. 14. The cumulative eigenvalue of each component in Fig. 13(a) indicates that the first three components account for approximately 99% of the overall FITR data set. Fig. 13(b) and (c) show a change in the score of each component as a function of exposure: the trend of the scores of PC1 and PC2 is similar to epoxy A, however, the change in the scores of PC1 and PC2 in epoxy B is more gradual. PC3 shows an increase in its score after the first exposure, and then starts to decrease. One again, PC1 offers the best means of differentiating the samples as a function of exposure. Fig. 13(d) shows the loading for each component and the results suggest that the function of each PC in epoxy B is similar to epoxy A. However, the change of several peaks varies since the two resin systems have different chemical structures and thus different stabilities.

In addition to the increasing intensity of OH deformation vibration in 1423 cm^{-1}, the C=O stretching vibration in 1740 cm^{-1} of epoxy B also increased due to the formation of C=O from carbonyl. The intensity of C=O stretching vibration from amide in 1660 cm^{-1} displays a gradual decrease due to the degradation of the amide group. Unlike epoxy A, epoxy B displays a significant decrease in 1039 cm^{-1}, due to the reaction between AO and the C–O–C group from ether, which will form C=O function group and increase the intensity of carbonyl in 1740 cm^{-1}. The C–Cl stretching vibration around 800 cm^{-1} also decreases due to degradation. Table 8 summarizes the trends in the changes in each peak in epoxy B with increasing AO fluence.

The PCA technique provides a more clear view of the FTIR data and the results suggest that the main changes occurring within the two resin systems include the significant degradation of the alkyl moieties, shifts in the position of the aromatic peaks, formation of OH and C=O groups, *etc.* The alkyl groups in both resins are almost complete degraded after the fifth exposure, which indicates that alkyl groups are the weak point within the structure. The shift of aromatic signals and formation of the OH and C=O functional groups indicate the abstraction and insertion mechanisms following the reaction with atomic oxygen.

4. Conclusions

In this study, the AO degradation behaviour of three thin laminates designed for space applications has been compared to understand the degradation mechanism of composite materials in LEO using PCA technique. The three laminates use two different epoxy resin systems and have comparable mechanical properties before exposure. The key findings of this work are that the mechanical tests suggest that the flexural properties of all laminates degrade after the first exposure due to the erosion of matrix. However, after the first exposure, the flexural properties will not change significantly unless the fibres become seriously eroded and damaged. The SEM images indicate that the resin on the surface of three laminates has been almost entirely eroded after AO exposure. Some residual resin remains in the gaps and at the edges of the carbon fibre yarn. The laminates experienced a gradual erosion of surface resin with the increase of AO fluence. A PCA analysis of the FTIR spectral data suggests that the surface resin on all laminates has suffered significant degradation after exposure, and that the alkyl moieties are the weak points of the structures since they are almost completely eroded after the fifth exposure, which is consistent with other researchers' work on the mechanism of AO erosion [11]. The application of the PCA method will assist with the future design of new matrix resins systems for this application, by gauging structural moieties in the molecular structure that are particularly susceptible to AO attack.

Author contributions

The manuscript was written through contributions of all authors. All authors have given approval for the final version of the manuscript.

Funding sources

The work of YH was supported by the Engineering and Physical Sciences Research Council through the EPSRC Centre for Doctoral Training in Advanced Composites for Innovation and Science [grant number EP/L016028/1] and a studentship (OSS).

Acknowledgments

We would like to acknowledge the Department of Physics (University of Bristol) for their support with the plasma asher facility. We are grateful to D. Griffin (University of Bristol) for help with the Matlab script.

Appendix A. Supplementary data

Supplementary data for this article can be found online at https://doi.org/10.1016/j.polymdegradstab.2019.05.026.

References

[1] Y. Gudimenko, R. Ng, J. Kleinman, Enhancement of space durability of materials and external components through surface modification, J. Spacecr. Rocket. 41 (3) (2004) 326–344.
[2] J.L. Barth, Space and Atmospheric Environments: from Low Earth Orbits to Deep Space, Springer, Netherlands, 2003.
[3] S. Samwel, Low Earth orbital atomic oxygen erosion effect on spacecraft materials, Space Res. J. 7 (1) (2014) 1–13.
[4] M. Dinguirard, J.C. Mandevillef, M. Van Eesbeek, A.P. Tighe, C. Durin, A. Chambers, S. Gabriel, D. Goulty, G. Roberts, Materials exposure and

degradation experiment (MEDET), in: Proceedings of the AIAA Space 2001 Conference and Exhibit on International Space Station Utilisation, Cape Canaveral, Florida, October 15-19, 2001, pp. 1–9.
[5] F. Imai, K. Imagawa, NASA's space environment exposure experiment on ISS – first retrieval of SM/MPAC & SEED, in: Materials in a Space Environment, vol. 540, 2003, pp. 589–594.
[6] D.E. Brinza, S.Y. Chung, T.K. Minton, R.H. Liang, Final Report on the NASA/JPL Evaluation of Oxygen Interactions with Materials – 3 (EOIM-3), NASA, 1994.
[7] K.K. De Groh, B.A. Banks, J.A. Dever, D.A. Jaworske, S.K. Miller, E.A. Sechkar, S.R. Panko, NASA glenn research center's materials international space station experiments (MISSE 1-7), Proceedings of the International Symposium on SM/MPACAC & SEED Experiment, Tsukuba, Japan, 10-11 March, 2008.
[8] Y. Kimoto, S. Ichikawa, E. Miyazaki, K. Matsumoto, J. Ishizawa, H. Shimamura, R. Yamanka, M. Suzuki, Space environment effects on materials at different positions and operational periods of ISS, in: AIP Conference Proceedings, AIP, 2009, 1087. No. 1.
[9] D.L. Edwards, A.P. Tighe, M. van Eesbeek, Y. Kimoto, K.K. de Groh, Overview of the natural space environment and ESA, JAXA, and NASA materials flight experiments, MRS Bull. 35 (2010) 25–34.
[10] G. Boocock, R.J. Cvetanovic, Reaction of oxygen atoms with benzene, Can. J. Chem. 39 (12) (1961) 2436–2443.
[11] R.A. Dressler, Chemical Dynamics in Extreme Environments, World Scientific, 2001.
[12] A. Suliga, E.M. Jakubczyk, I. Hamerton, I.,A. Viquerat, Analysis of atomic oxygen and ultraviolet exposure effects on cycloaliphatic epoxy resins reinforced with octa-functional POSS, Acta Astronaut. 142 (2018) 103–111.
[13] J.R. Reveles, M. Lawton, V. Fraux, V. Gurusamy, V. Parry, SSC17-II-08 In-Orbit Performance of AstroTube™: AlSat Nano's Low Mass Deployable Composite Boom Payload,, in: Small Satellite Conference, Logan, Uha, USA, August 2017.
[14] T.W. Murphey, W. Francis, B. Davis, J.M. Meja-Ariza, High Strain Composites, *2nd AIAA Spacecraft Structures Conference*, Kissimmee, Florida, 5-9 January 2015.
[15] G.L. Steckel, T. Cookson, C. Blair, LDEF materials workshop '91. B.A. Stein and P.R. Young (compilers), NASA CP- 3162 (2) (1992) 515.
[16] A.S. Levine (Ed.), *Third LDEF post-retrieval symposium*, LDEF science office, NASA Langley Research Centre and American Institute of Aeronautics and Astronautics, Williamsburg Lodge, Williamsburg VA 23185, NASA CP 10120, 1993. November 8-12, 1993.
[17] Y. Gudimenko, R. Ng, J. Kleiman, Z. Iskanderova, P.C. Hughes, R.C. Tennyson, D. Milligan, Photosil™ surface modification treatment of polymer-based space materials and external space components, in: Protection of Materials and Structures from Space Environment. Springer, Dordrecht, 2004, pp. 419–434.
[18] C.A. Arnold, J.D. Summers, J.E. McGrath, Synthesis and physical behavior of siloxane modified polyimides, Polym. Eng. Sci. 29 (1989) 1413.
[19] S.H. Phillips, T.S. Haddad, S.J. Tomczak, Developments in nanoscience: polyhedral oligomeric silsesquioxane (POSS)-polymers, Curr. Opin. Solid State Mater. Sci. 8 (1) (2004) 21–29.
[20] F. Awaja, J.B. Moon, M. Gilbert, S. Zhang, C.G. Kim, P.J. Pigram, Surface molecular degradation of 3D glass polymer composite under low earth orbit environmental conditions, Polym. Degrad. Stabil. 95 (2010) 987–996.
[21] F. Awaja, J.B. Moon, M. Gilbert, S. Zhang, C.G. Kim, P.J. Pigram, Surface molecular degradation of selected high performance polymer composites under low earth orbit environmental conditions, Polym. Degrad. Stabil. 96 (2011) 1301–1309.
[22] Cytec Advanced Composites Group, MTM 44-1 Data Sheet. https://www.cytec.com/sites/default/files/datasheets/MTM44-1.pdf. (Accessed 20 January 2019).
[23] Cytec Advanced Composites Group, MTM 49-3 Data Sheet. https://cytec.com/sites/default/files/datasheets/MTM49.pdf. (Accessed 20 January 2019).
[24] K.K. de Groh, B.A. Banks, C.E. McCarthy, R.N. Rucker, L.M. Roberts, L.A. Berger, MISSE PEACE Polymers Atomic Oxygen Erosion Results, NASA, 2006.
[25] ASTM International, Standard Test Methods for Flexural Properties of Unreinforced and Reinforced Plastics and Electrical Insulating Materials. D790, Annual Book of ASTM Standards, 2002, pp. 1–12.
[26] C. Zweben, W.S. Smith, M.W. Wardle, Test methods for fiber tensile strength, composite flexural modulus, and properties of fabric-reinforced laminates, Compos. Mater.: Testing and Design (Fifth Conference) 674 (1979) 228–262.
[27] F. Gaston, N. Dupuy, S.R. Marque, M. Barbaroux, S. Dorey, FTIR study of ageing of γ-irradiated biopharmaceutical EVA based film, Polym. Degrad. Stabil. 129 (2016) 19–25.
[28] P. He, Y. Xiao, P. Zhang, C. Xing, N. Zhu, X. Zhu, D. Yan, Thermal degradation of syndiotactic polypropylene and the influence of stereoregularity on the thermal degradation behaviour by *in situ* FTIR spectroscopy, Polym. Degrad. Stabil. 88 (3) (2005) 473–479.
[29] H. Pan, X. Qian, L. Ma, L. Song, Y. Hu, K.M. Liew, Preparation of a novel bio-based flame retardant containing phosphorus and nitrogen and its performance on the flame retardancy and thermal stability of poly (vinyl alcohol), Polym. Degrad. Stabil. 106 (2014) 47–53.
[30] H.S.P. Da Silva, H.L. Ornaghi Júnior, J.H. Santos Almeida Júnior, A.J. Zattera, S. Campos Amico, Mechanical behavior and correlation between dynamic fragility and dynamic mechanical properties of curaua fiber composites, Polym. Compos. 35 (2014) 1078–1086.
[31] L. Mooring, S. thompson, S.A. Hall, S. Pani, P. Zioupos, M. Swan, C. Stone, B.J. Howlin, I. Hamerton, 'Phoenix polymers': fire induced nanohardness in fibril-forming aromatic cyanate esters, RSC Adv. 8 (2018) 36264–36271.